

Search of MeV-GeV counterparts of TeV sources with AGILE in pointing mode

A. Rappoldi¹*, F. Lucarelli^{2,3}, C. Pittori^{2,3}, F. Longo^{4,5}, P.W. Cattaneo¹, F. Verrecchia^{2,3}, M. Tavani^{6,7}, A. Bulgarelli⁸, A.W. Chen⁹, S. Colafrancesco⁹, I. Donnarumma⁶, A. Giuliani¹⁰, A. Morselli¹¹, S. Sabatini⁶, and S. Vercellone¹²

¹ INFN-Pavia, via Bassi 6, I-27100 Pavia, Italy

² ASI Science Data Center, via del Politecnico snc 00133, Roma, Italy

³ INAF-Osservatorio Astronomico di Roma, via di Frascati 33, I-00040 Monteporzio Catone, Roma, Italy

⁴ INAF-Osservatorio Astronomico di Trieste, via G.B. Tiepolo 11, I-34143 Trieste, Italy

⁵ INFN-Trieste, Padriciano 99, I-34012 Trieste, Italy

⁶ INAF-IAPS Roma, via Fosso del Cavaliere 100, I-00133 Roma, Italy

⁷ Dip. di Fisica, Università “Tor Vergata”, via della Ricerca Scientifica 1, I-00133 Roma, Italy

⁸ INAF-IASF Bologna, via Gobetti 101, I-40129 Bologna, Italy

⁹ School of Physics, University of the Witwatersrand, Johannesburg Wits 2050, South Africa

¹⁰ INAF-IASF Milano, via E. Bassini 15, I-20133 Milano, Italy

¹¹ INFN-Roma Tor Vergata, via della Ricerca Scientifica 1, 00133 Roma, Italy

¹² INAF-IASF Palermo, Via Ugo La Malfa 153, I-90146 Palermo, Italy

Abstract

Context. Known TeV sources detected by major Čerenkov telescopes are investigated to identify possible MeV-GeV γ -ray counterparts.

Aims. A systematic study of the known sources in the web-based *TeVCat* Catalog has been performed to search for possible γ -ray counterpart on the AGILE data collected during the first period of operations in observing pointing mode.

Methods. For each TeV source, a search for a possible γ -ray counterpart based on a multi-source Maximum Likelihood algorithm is performed on the AGILE data taken with the GRID instrument from July 2007 to October 2009.

Results. In case of high-significance detection, the average γ -ray flux is estimated. For the cases of low-significance detection the 95% Confidence Level (C.L.) flux upper limit is given. 52 TeV sources out of 152 (corresponding to $\sim 34\%$ of the analysed sample) show a significant excess in the AGILE data covering the pointing observation period.

Conclusions. This analysis found 26 new AGILE sources with respect to the AGILE reference catalogs, 15 of which are Galactic, 7 are extragalactic and 4 are unidentified. Detailed tables with all available information on the analysed sources are presented.

Key words. catalogs – γ -rays: general

1. Introduction

In the last years, the number of identified TeV sources has increased up to more than 100, thanks to the observations made by the new generation of ground-based Čerenkov telescopes HESS (Hinton 2004), MAGIC (Ferenc 2005) and VERITAS (Holder et al. 2006). These sources mainly belong to five classes: Active Galactic Nuclei (AGN), Supernova Remnants (SNR), Pulsar Wind Nebulae (PWN), X-rays binary systems (XRB), and Pulsars (PSR). More than 80 TeV sources are Galactic and a significant fraction of them ($\gtrsim 20\%$) does not show any evident counterpart and remains unidentified (UNID).

Multi-wavelength deep observations of the regions near the TeV sources are needed to identify the possible counterparts of the UNID, as well as to understand the emission mechanisms of the TeV γ -rays.

Following previous studies on positional and spectral connection of GeV to TeV γ -ray sources done for EGRET and Fermi LAT (Funk et al. 2008, 2013; Abdo et al. 2009; Acero et al. 2013), this paper reports the results of the

search for γ -ray emission from known and unidentified TeV sources, using the data collected by AGILE in pointing mode in the energy range above 100 MeV.

This search is particularly relevant, as demonstrated by the previous studies, due to the fact that two adjacent energy ranges probe different regions of the source spectra. Preliminary results have been previously presented (Rappoldi et al. 2011; Longo et al. 2011).

2. The TeV source Catalog

The analysis described in this paper has been applied to a reference sample of TeV sources extracted from the on-line *TeVCat* Catalog¹ (Wakely, S. and Horan, D.). This on-line catalog is continuously updated with new sources detected by the TeV experiments, and for each source it provides many parameters such as coordinates, source type, flux and estimated distance (when available).

At the time of writing (June 2015), the *TeVCat* Catalog contains a total of 183 TeV sources: 129 of those are flagged

* Corresponding author

¹ <http://tevcatalog.uchicago.edu/>

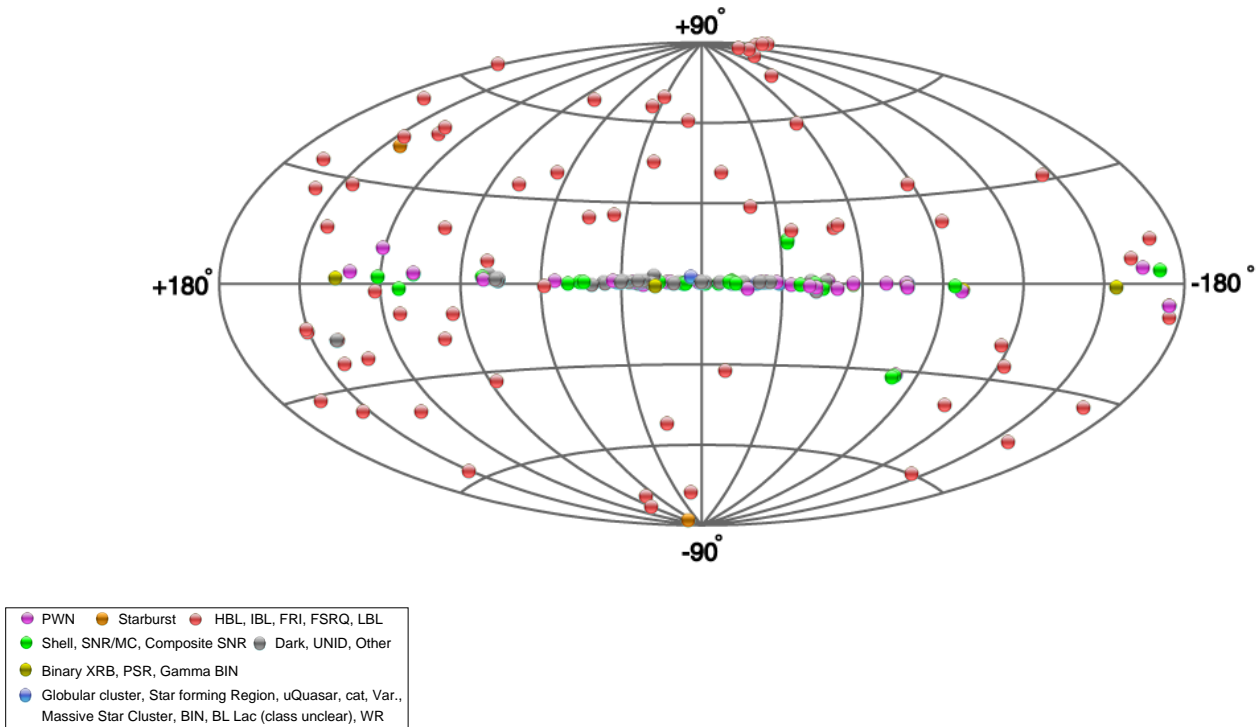


Figure 1. The Aitoff projection in Galactic coordinates of the TeV source positions, as extracted from the on-line *TeVCat* (*Default Catalog* and *Newly Announced* samples, June 2015) (Wakely, S. and Horan, D.).

as *Default Catalog* and have been published on refereed journals, 32 are flagged as *Newly Announced* (see also Fig. 1), 10 are flagged as *Other Sources* and 12 are flagged as *Sources Candidates*. The analysis described here was performed on a subset of 152 TeV sources, both Galactic and extragalactic, consisting of 120 sources of the *Default Catalog*, plus 32 *Newly Announced* sources. The following criteria were adopted to define the input sample. Three *extended regions*, which already include a compact TeV source, were excluded: the Galactic Centre Ridge (including HESS J1745-290 and SNR G 0.9+0.1), Boomerang PWN (including SNR G 106.3+2.7) and Milagro Diffuse (including MGRO J2019+37). The TeV sources SN 1006 SW and NE, HESS J1018-589 A and B as well as HESS J1800-240 A and B, were considered as single candidate γ -ray sources located, respectively, at the centre of the SNR 1006 shell, and at the centroid positions of HESS J1018-589 and HESS J1800-240. The two TeV sources ARGO J2031+4157 and MGRO J2031+41 were not included since they are both associated with TeV J2032+415 in the *TeVCat*. Moreover, the detection of the pulsed emission at TeV energies from the Crab and Vela Pulsar has been not considered in the sample since the timing analysis of pulsars is out of the scope of this paper.

Each sky position and extension of the TeV sources in the selected *TeVCat* sample has been carefully reviewed using published data. A new interactive web page of the catalog of TeV sources, including this coordinate revision and giving public access to light curves and spectra, is now available at the ASI Science Data Center (ASDC) (Carosi et al. in press 2015)².

When available, the best-fit position of the TeV excess has been used as starting input position for the AGILE data analysis. Otherwise, the position of the optical/radio known counterpart has been used. The error region on each TeV

source position has been calculated by summing quadratically the statistical uncertainties on the position coordinates obtained from the 2D-Gaussian fit of the TeV excess, and the systematic uncertainties on the instrument pointing (when available in the literature).

3. The AGILE satellite

AGILE (Tavani et al. 2009) is an Italian Space Agency (ASI) small scientific mission for high-energy astrophysics launched on April 23, 2007 from the Indian base of Sriharikota in an equatorial orbit optimised for low particle background, with a very small inclination angle ($\sim 2.5^\circ$) and initial altitude of about 550 km.

The analysis has been performed using the data collected by the main AGILE instrument, the *Gamma-Ray Imaging Detector* (GRID). The AGILE-GRID is sensitive in the energy range 30 MeV – 50 GeV, and it consists of a silicon-tungsten tracker, a caesium iodide mini-calorimeter and an anticoincidence system made of segmented plastic scintillators. The use of the silicon strip technology allows to have good performance for the γ -ray GRID imager, approximately a small cube of ~ 60 cm size, which achieves an effective area of the order of 500 cm² at several hundreds MeV, an angular resolution (at 68% containment radius) of about 4.3° at 100 MeV, decreasing below 1° for energies above 1 GeV (Chen et al. 2013), an unprecedentedly large field of view (FOV) of about ~ 2.5 sr, as well as accurate timing, positional and attitude information (source location accuracy 5' – 10' for intense sources with $S/N \gtrsim 10$).

4. AGILE data set

During its first period of data taking (about two years) the AGILE satellite was operated in “pointing observing mode”, and the corresponding AGILE data are divided in

² <http://www.asdc.asi.it/tevcats/>

Observation Blocks (OBs). Each AGILE OBs consists of long exposures, which mostly range from a few days to about thirty days, with the pointing direction drifting $\sim 1^\circ$ per day with respect to the initial boresight direction to match solar panel illumination constraints.

The analysed AGILE data set covers the period from July 9, 2007 (beginning of the science verification phase) to October 18, 2009, corresponding to 96 OBs (not including the first 5 OBs of the Commissioning). During this period, following the main scientific program of the AGILE mission, the satellite was mainly pointed to observe two regions near the Galactic Plane, around $l = 90^\circ$ and $l = 270^\circ$ longitude values, as shown by the total exposure map in Fig. 2. Clearly, this observation strategy mainly focused on the Galactic plane was not optimal for detecting extragalactic TeV sources.

5. Data analysis procedure

An iterative automated procedure has been developed to analyse the entire pointing AGILE data set described in Sec. 4, searching for possible γ -ray excesses correlated to the TeV sources. For each TeV source in the reference sample defined in Sec. 2, this procedure is divided in two main parts.

5.1. Maps creation

The first part consists in the creation of the maps of counts, exposure and diffuse γ -ray background based on the model described in (Giuliani et al. 2004) updated together with the new GRID Calibrations, centred at the TeV source position, over the full AGILE pointed observation period. These maps are in Galactic coordinates (l , b), ARC projection, with size of $40^\circ \times 40^\circ$ divided in bins of $0.1^\circ \times 0.1^\circ$, and they have been produced using the latest official AGILE scientific analysis software (Chen et al. 2011) – available at ASDC – with the following parameters:

- *data archive*: ASDCSTDe
- *initial time*: MJD (TT) = 54290.5 (MET=111067134 s)³
- *final time*: MJD (TT) = 55122.5 (MET=182951934 s)
- *energy range*: 100 MeV ÷ 50 GeV
- *software release*: BUILD21
- *event filter*: FM3.119
- *response matrices*: I0023

The *event filter* is the algorithm that processes the GRID raw data and reconstructs the energy and direction of the incident γ -ray in the GRID reference system. The event filter used in this analysis (FM3.119) represents the most updated reconstruction algorithm, which provides a good trade-off between FoV, effective area and background rejection (Chen et al. 2011, 2013). Maps were generated for energies $E > 100$ MeV, including all events collected up to 60° off-axis. The South Atlantic Anomaly data were excluded, and to eliminate the Earth albedo contamination, events with reconstructed directions with respect to the satellite-Earth vector smaller than 85° were also rejected.

5.2. Source detection

The next part of the automatic procedure consists in verifying if around the input TeV position it is possible to detect

³ MET is the AGILE Mission Elapsed Time in seconds since 2004.0 UTC.

the presence of a significant γ -ray source and, if so, to try to locate the best position of the γ -ray excess.

The source detection is performed by means of a *multi-source* Maximum Likelihood Estimator (MLE) algorithm that estimates the photon counts and the position of the TeV source, the expected contribution given by the background components (modelled as a superposition of a Galactic diffuse emission background and an isotropic component), all the known AGILE γ -ray sources within the region of analysis, taking also into account the instrument response function.

In particular, the MLE analysis was performed taking into account all the known γ -ray sources detected by AGILE at the time of the analysis, consisting of a set of 65 sources, obtained by combining the 54 sources of the updated list of AGILE bright sources (1AGLR; Verrecchia et al. 2013), plus 11 sources not bright enough to be detected over the short OB time scales of the 1AGLR analysis: i.e. eight 1AGL sources from the first AGILE high confidence Catalog (Pittori et al. 2009) and two AGL sources in the Carina region (see also Tab. 2 and Tab. 3 of 1AGLR paper), plus one additional AGL source from a detailed analysis of the Cygnus region (Bulgarelli et al. 2012b). All AGILE sources are assumed to be point-like with simple power-law spectra.

With the exception of bright sources (significance > 5), AGILE data analysis may not be spectrally resolved due to low statistics, and in general a standard fixed spectral index value of -2.1 is adopted for the initial steps of the ML analysis. This assumption is motivated by the known spectral properties of the majority of the γ -ray sources in the AGILE energy range, except for few sources as described in the 1AGLR. Timing analysis of pulsars was not performed in this paper, and the γ -ray emission detected in the search of counterparts to the TeV emission from PWN is in general due to the average (pulsar + nebula) γ -ray flux values.

The significance of a source detection is evaluated by the square root of the *test statistic* TS , defined as

$$TS = -2 \log \left(\frac{\mathcal{L}_0}{\mathcal{L}_1} \right) \quad (1)$$

where $\mathcal{L}_0/\mathcal{L}_1$ is the ratio between the maximum likelihood \mathcal{L}_0 of the null hypothesis and the likelihood \mathcal{L}_1 of the alternative hypothesis (presence of a point-like source under evaluation) (Mattox et al. 1996; Bulgarelli et al. 2012a). For a large enough number of counts ($N \gtrsim 20$), TS is expected to behave as χ_1^2 in the null hypothesis, and the significance of a source detection is given by \sqrt{TS} .

The source detection algorithm is very flexible and can be used with a variety of parameters and options that allow to refine the process of source detection and location. For example, both the position and the flux of the analysed source can be considered fixed or variable (starting from a defined initial value), as well as the coefficients of the Galactic background (diffuse emission and isotropic component) may in turn be kept fixed or treated as variable.

In order to get the best result for the position and flux estimation of the analysed sources, an iterative MLE analysis is performed, divided into the following steps:

- **step 1**: the aim of the first step is both to find an excess of γ -rays around the input TeV source position in the AGILE data, and to estimate by the minimisation algorithm the best values of the γ -ray background model parameters (Galactic and extragalactic isotropic contributions). The MLE analysis is performed allowing the

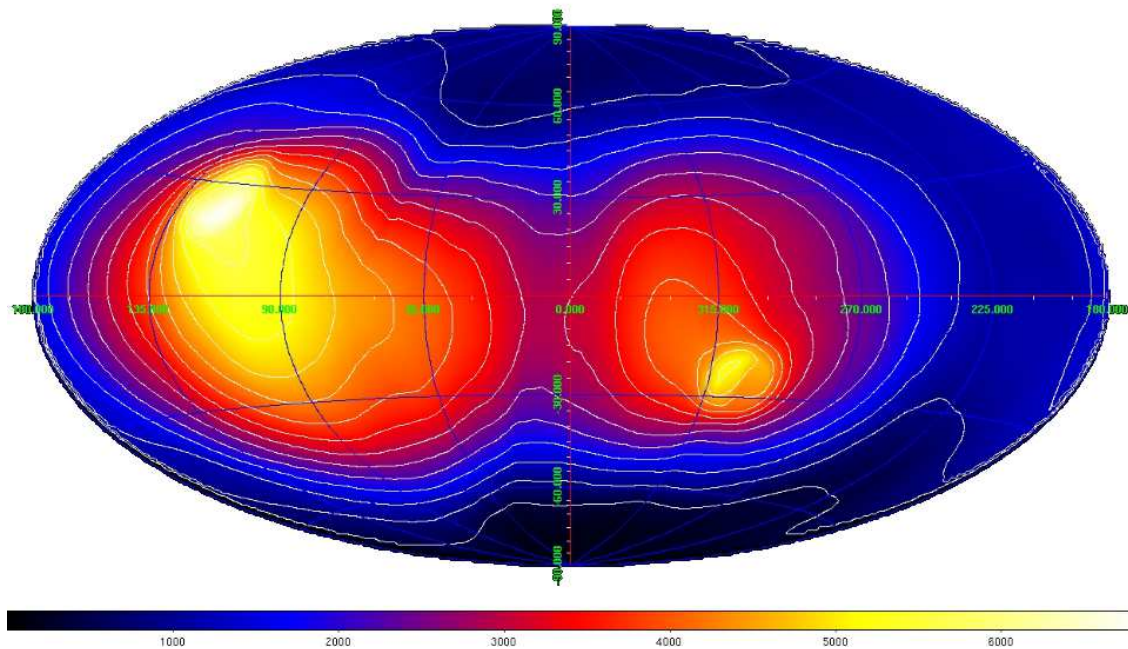


Figure 2. Total AGILE exposure map during the first \sim two years of operations (July 2007 – October 2009). The exposure values are expressed in $[\text{cm}^2 \text{ Ms}]$. The mean, maximum and minimum exposures attained correspond to values of about 2250, 6800 and 60 $\text{cm}^2 \text{ Ms}$, respectively.

source coordinates to vary within a distance $\leq 1^\circ$ from the input TeV source position, taking into account all known AGILE sources in the region of analysis with a radius of 10° ;

- **step 2:** in this step the γ -ray excess position is refined by fixing the Galactic background coefficients to the best values obtained from step 1;
- **step 3:** this is the final step to estimate the flux and significance $\sqrt{(TS)_3}$ of the γ -ray source at the optimised position resulting from step 2, using updated Galactic background coefficients at the new position;
- **step 4:** this step gives directly an estimation of the flux and significance $\sqrt{(TS)_4}$ of the γ -ray source assuming a fixed position coincident with that of the input TeV source. In this case the diffuse background coefficients are estimated at the original input position.

Step 4 represents the standard method used in literature to verify the significance of known sources at input positions already known in other wavelengths. However, especially in the analysis of crowded regions of the Galactic plane, it is important also to search for a possible optimised position of the γ -ray excess, still compatible with the TeV source spatial association. This search is performed in *step 1 – step 3*.

The possible shift in the γ -ray excess position may be due to several factors:

- the rather poor angular resolution of the order of a few degrees in the MeV–GeV energy range⁴;
- the AGILE reference catalogs positioning errors (ranging from $\sim 0.1^\circ$ for very bright sources up to 0.7° for faint sources, at 95% C. L.);

⁴ About 0.7° PSF HWHM at 400 MeV, corresponding to the AGILE effective area peak values (Sabatini et al. 2015).

- extended TeV source (X);
- the possible physical displacement between the TeV and the MeV–GeV emission regions.

In this paper an AGILE *detection* is in general defined by the condition:

$$\sqrt{(TS)_4} \geq 4 \quad (2)$$

which corresponds to a statistical significance of about 4σ at the input TeV source position.

The search for optimised positions of the γ -ray excess gives results which are considered reliable when the MLE analysis (*step 1 – step 3*) converges well within the allowed searching distance from the input position, and the significance of the detection is increased. In practice (see next section) when the following condition is satisfied:

$$\sqrt{(TS)_3} \geq 4 \text{ and } \text{and } dist \lesssim 0.6^\circ \quad (3)$$

where *dist* is the angular distance between the position of the input TeV source and the candidate γ -ray source.

6. Results

In Tab. 1 the complete list of all the TeV sources considered in this analysis is reported, showing the following relevant source parameters:

- ID: identification number;
- TeV source: TeV source name;
- (l,b): position of the TeV source in Galactic Coordinates;
- TeV Pos. Err.: positional error of the input TeV source (derived as explained in Sec. 2);
- Canonical name;
- Type: type of TeV source counterpart, if already known from other wavelengths;
- $\sqrt{(TS)_4}$: estimate of the γ -ray statistical significance at *step 4*;

- $\sqrt{(TS)_3}$: estimate of the γ -ray statistical significance at *step 3*;
- Flux₄: estimate of the γ -ray flux ($E > 100$ MeV) and its 1σ statistical error in units of 10^{-7} ph cm $^{-2}$ s $^{-1}$, for AGILE detected sources at the input TeV source position from *step 4*;
- UL₄: AGILE γ -ray flux upper limit at 95% C.L. at the input TeV source position from *step 4*;
- EXT: TeV source extension.

In Tab. 1 the γ -ray sources detected according to the criteria specified in Sec. 5.2 are shown in bold. For these sources the calculated flux value and the corresponding error is given, while for the sources not satisfying the detection requirement, the estimated 95% C.L. upper limit is reported.

In total, 52 TeV sources show a significant excess in the AGILE data covering the pointed observation period, corresponding to 34% of the original sample. The Aitoff map in Galactic coordinates of all the detections is shown in Fig. 3.

Tab. 2 groups all the sources detected with AGILE in this work (shown in bold in the previous table), and it includes the following columns:

- ID: source identification number used in Tab. 1
- TeV Source: TeV source name;
- $\sqrt{(TS)}$: estimate of the γ -ray source statistical significance as result of the AGILE MLE analysis (upper part *step 3*, lower part *step 4*);
- (l,b): optimised peak position of the AGILE excess in Galactic Coordinates (upper part);
- Error: γ -ray source location error radius at 95% C.L. from *step 3* (statistical error only);
- Flux: estimate of the γ -ray flux ($E > 100$ MeV) at the optimised peak position and its 1σ statistical error in units of 10^{-7} ph cm $^{-2}$ s $^{-1}$;
- Dist: distance of the γ -ray peak position from the input position of the TeV source;
- AGILE association: already known AGILE source from the published 1AGL/1AGLR catalogs (Pittori et al. 2009; Verrecchia et al. 2013) within the error radius in the 7th column;
- Fermi association: known Fermi-LAT source(s) associated to the TeV source, as described on 3FGL Catalog (Acero et al. 2015);
- Analysis flag (see below).

Tab. 2 is split in two sections: the upper part reports the results of MLE analysis *step 3* for all the sources satisfying the condition in Eq. (3). The lower part includes the detected sources satisfying the condition in Eq. (2) but not Eq. (3), for which the *step 3* automatic analysis is not reliable. For this reason, the values of \sqrt{TS} and flux shown in this part of the table are those found at *step 4* at the input TeV positions. There are few exceptions to these criteria which are described in the table footnotes. For all the 19 sources in the lower section of Tab. 2, although the MLE analysis result at fixed input position is significant, the tentative optimisation of the location of the γ -ray peak flux fails. In this cases the region of analysis may be not yet well modelled, and a refined MLE analysis should be performed after the release of new AGILE Catalog (Bulgarelli et al., in preparation).

As reported in the 8th column of Tab. 2, 26 spatial associations of the detected TeV sources with already known AGILE sources from the the 1AGL/1AGLR catalogs are found within the 95% C.L. error radius (7th column) (Pittori et al. 2009; Verrecchia et al. 2013). Among

these sources, 15 are Galactic, 6 are extragalactic and 5 are unassociated. As reported in the 9th column, 46 spatial associations with known Fermi sources from the 3FGL Catalog are found (note that some TeV sources have more than one 3FGL association). Fermi counterparts officially associated in the 3FGL Catalog to the corresponding TeV source may have flag P (for point-like sources) or E (for extended sources).

Column 10th of Tab. 2 reports an analysis flag assigned to the AGILE detection according to the position and extent of the source location contour:

- *IN* (Inside): the TeV source, including its extension (if any), is entirely within the AGILE contour (see an example in Fig. 4);
- *O* (*Overlapping*): the AGILE contour at the 95% C.L. overlaps with the error circle and/or the extension of the TeV source (see Fig. 5);
- *E* (*External*): the AGILE contour neither includes nor overlaps with the TeV source. Nevertheless, the AGILE peak position is within 0.6° from the TeV source position (see Fig. 6).

In this work 26 new AGILE sources are found with respect to the AGILE reference catalogs, 15 of which are Galactic, 7 are extragalactic and 4 are unidentified. A detailed statistics about the type of the detected source can be found in Tab. 4.

There are 8 sources detected by AGILE in this analysis with no Fermi 3FGL official association:

- * ID 88: TeV J1634-472 (HESS J1634-472)
- ID 96: TeV J1713-382 (CTB 37B)
- ID 103: TeV J1729-345 (HESS J1729-345)
- ID 104: TeV J1732-347 (HESS J1731-347)
- ID 105: TeV J1741-302 (HESS J1741-302)
- * ID 116: TeV J1813-178 (HESS J1813-178)
- ID 133: TeV J1911+090 (W49B)
- ID 134: TeV J1912+101 (HESS J1912+101)

two of which, indicated by asterisks, have counterparts in the already published AGILE catalogs, and do not represent new detections.

6.1. Spectral analysis

Tab. 3 shows the results of the spectral analysis performed on the most significant sources detected in this analysis. Only the 24 sources detected with a significance $\sqrt{(TS)_3} > 5$ (see Tab. 2, upper part) and $|b| < 30^\circ$ have been considered.

For all considered sources, the AGILE spectral index shown in the fourth column of Tab. 3 has been calculated generating exposure, counts and diffuse background maps over five energy bands: 100–200 MeV, 200–400 MeV, 400–1000 MeV, 1–3 GeV and 3–50 GeV, under the assumption of a power-law energy distribution.

For comparison, the Fermi power-law spectral index of the 3FGL counterpart of the TeV source is also shown in the last column of the table⁵. AGILE and Fermi power-law spectral indices are also compared in Fig. 7. A quantitative comparison between Fermi and AGILE power-law spectral

⁵ The *power law index* reported on 3FGL Catalog (Acero et al. 2015) is given without error, and corresponds to the result of fitting the spectrum with a power-law function; it is equal to *Spectral Index* only when spectrum type is `PowerLaw` and in these cases errors are available.

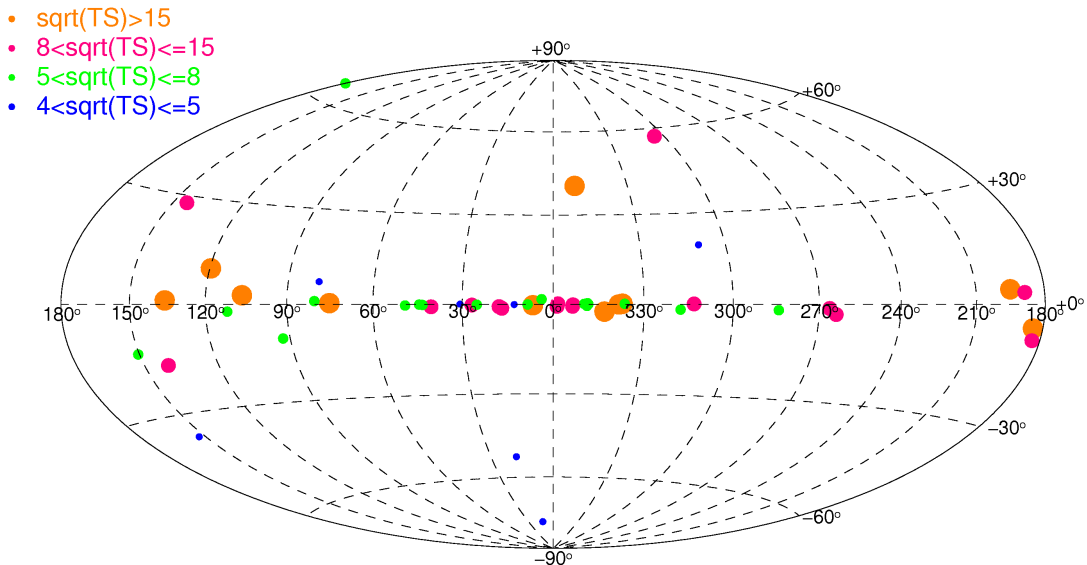


Figure 3. Aitoff map in Galactic coordinates of all the detections according to the criteria specified in the text, corresponding to TeV sources showing a significant excess in the AGILE data.

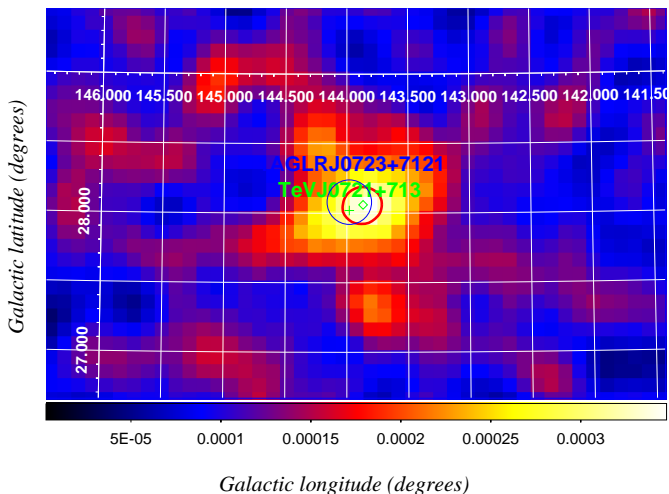


Figure 4. Source detection in the position of TeV J0721+713. The signal is detected with $\sqrt{(TS)_3} = 13.9$, and the localization algorithm gives the 95% C.L. contour (red curve) that entirely contains the TeV source position (green cross). The AGILE counterpart 1AGLR J0723+7121 is also shown with its error radius (blue circle). The picture shows the *intensity* map ($\text{cm}^{-2}\text{s}^{-1}\text{bin}^{-1}$) in galactic coordinates, with bin size $0.1^\circ \times 0.1^\circ$ and Gaussian smoothing of three bins' radius.

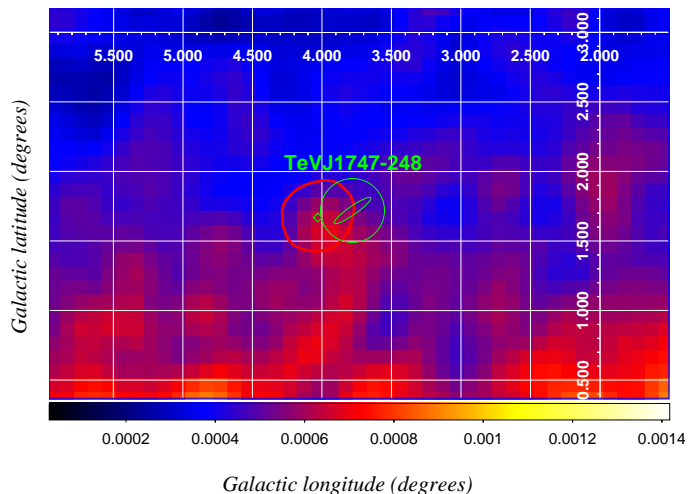


Figure 5. Source detection in the position of TeV J1747-248. The signal is detected with $\sqrt{(TS)_3} = 5.9$, and the localization algorithm gives the 95% C.L. contour (red curve) which partially overlaps with the error circle and the extension of the TeV source (green circle and green ellipse). The picture shows the *intensity* map ($\text{cm}^{-2}\text{s}^{-1}\text{bin}^{-1}$) in galactic coordinates, with bin size $0.1^\circ \times 0.1^\circ$ and Gaussian smoothing of three bins' radius.

indices can be done adding quadratically the AGILE and Fermi power-law spectral index errors when available or relying only on the AGILE error. No systematic error is assumed. On these very conservative assumptions the distribution of the pulls (difference between the AGILE and Fermi power-law spectral indices divided by their combined errors) shown in Fig.8 can be significantly overestimated. Nevertheless, for most of the sources (19 out of 22), AGILE and Fermi power-law spectral indices agree within three σ .

As explained in Section 5.2, the analysis in this paper was performed taking into account all the known γ -ray

sources detected by AGILE at the time of the analysis, and in general more than one 3FGL source may be within the 95% AGILE error circle (plus a suggested systematic error of 0.1°). In particular in the TeV J1841-055 case, the one with the largest pull (red), there are three 3FGL sources within the AGILE detection error circle. The TeV source has an extension of the order of 0.5 degrees, and the AGILE spectral result was compared with the associated extended Fermi PWN 3FGL J1840.9-0532e. It is likely that other two γ -ray sources (3FGL J1839.3-0552 and 3FGL J1838.9-0537) contribute to the AGILE detected emission, both having softer power-law spectral indices.

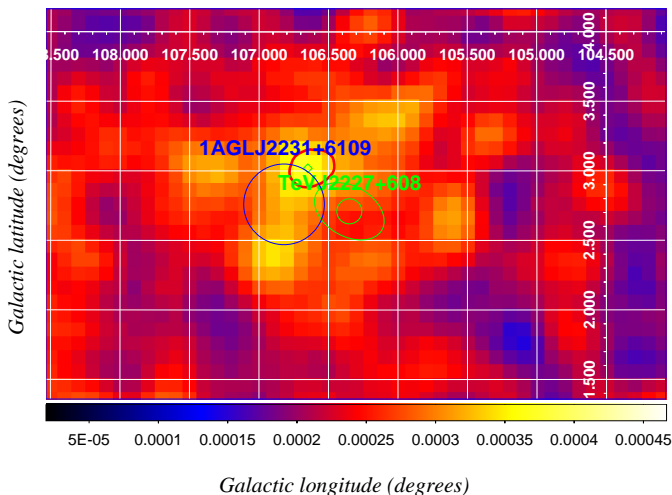


Figure 6. Source detection in the position of TeV J2227+608. The signal is detected with $\sqrt{(TS)_3} = 16.7$, and the localization algorithm gives the 95% C.L. contour (red curve) which neither includes nor overlaps with the error circle and the extension of the TeV source (green circle and green ellipse). The AGILE counterpart 1AGL J2231+6109 is also shown with its error radius (blue circle). The picture shows the *intensity* map ($\text{cm}^{-2}\text{s}^{-1}\text{bin}^{-1}$) in galactic coordinates, with bin size $0.1^\circ \times 0.1^\circ$ and Gaussian smoothing of three bins' radius.

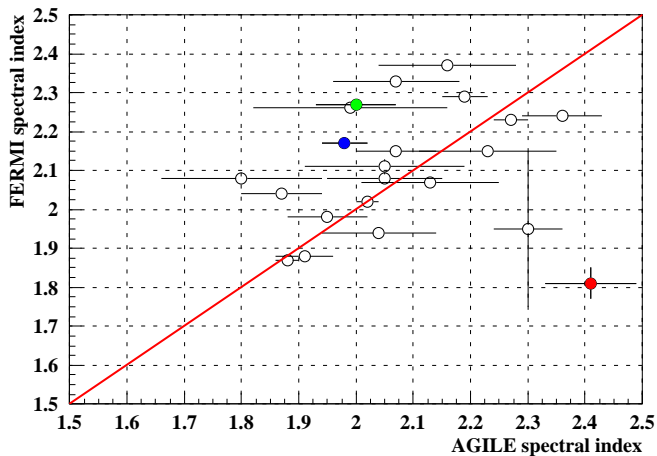


Figure 7. Comparison between the spectral index evaluated for the most significant sources detected by AGILE, and the corresponding *power-law* spectral index reported by Fermi (22 sources). The horizontal bars represent the AGILE spectral index errors, the vertical bars represent the Fermi spectral index errors, when available. The coloured points refer to the sources highlighted in Fig. 8

7. Conclusions and discussion

An analysis has been performed on a sample of 152 known TeV sources using the first two years of AGILE data, with the purpose to detect γ -ray emission associated with these TeV sources.

A significant γ -ray excess in the AGILE data has been found for 52 input TeV sources, corresponding to $\sim 34\%$ of the analysed sample. In particular 26 new AGILE sources have been found with respect to the AGILE reference cata-

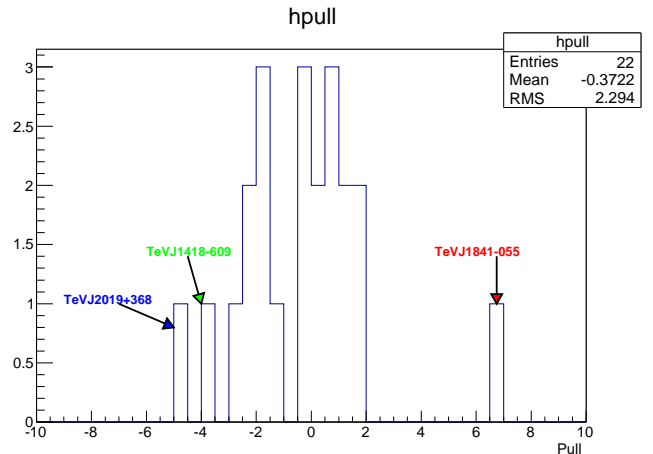


Figure 8. Pull distribution of the difference between the AGILE and Fermi power-law spectral indices divided by their combined errors. The three sources with pull larger than three are shown.

logs, 15 of which are Galactic, 7 are extragalactic and 4 are unidentified.

Eight of the AGILE detected TeV sources (listed in Sect. 6) have no 3FGL official association and will be further investigated in a dedicated paper.

The difference between the two experiments in some cases may be due to a different response to softer spectral index sources with spectral energy distribution peaking in the 100-400 MeV energy range or to differences in the assumed background diffuse model. A new Fermi analysis using the recently delivered “Pass 8 Data” providing a significant increase in acceptance at lower energies may result in new Fermi associations. Furthermore according to the official Fermi collaboration association procedure, only counterparts which reach a posteriori probability of at least 80% are retained, and this does not mean that there is no 3FGL source within the error region.

The spatial association of a TeV source with an AGILE source may be due to chance. The probability of serendipitous association may be estimated evaluating the total sky coverage of all catalogued AGILE sources, defined by their 95% error radius, and then calculating the overall probability that each TeV source can overlap to any AGILE source, that is, the distance between a TeV source and an AGILE source is by chance smaller than the sum of their error circles (Funk et al. 2007). Because of the density of both TeV and AGILE sources are strongly non uniform, being much larger on the Galactic plane, this evaluation is performed separately on a narrow stripe along the Galactic plane⁶, defined by $|b| \leq 3^\circ$, and on all the rest of the sky map, defined by $|b| > 3^\circ$. The number of serendipitous associations is found to be 0.82 for such a band around the Galactic plane, whereas it is 0.08 for the other region. Therefore the chance coincidence should be $\mathcal{O}(1)$ over all the sky.

It is worth noting that the analysis accomplished and described in this paper concerns a nearly continuous data taking period of about 2 year, therefore the obtained fluxes (and corresponding detection significances) are the average values integrated over a rather long time. For this reason, some γ -sources characterised by high variability (for example W Comae (Verrecchia et al. 2008) and 4C +21.35

⁶ The probability estimation is weakly dependent on the boundary used.

(Bulgarelli et al. 2010; Striani et al. 2010; Verrecchia et al. 2014)) has not been detected in this analysis (and similarly in Verrecchia et al. 2013), even if they have already been detected and analysed in other previous observations published by AGILE, referring to shorter time periods in coincidence with their flares.

The majority of the AGILE detected sources are Galactic. This might be a bias due to the higher exposure of the Galactic Plane during the Pointing period, see Fig. 2.

From the “Analysis flag” reported in Tab. 2, there are 13 AGILE detected sources in the Galactic plane flagged as “Overlapping” or “External” with the TeV emission region. This may indicate a possible displacement between the TeV and the GeV emission regions, as it is the case for the IC443 SNR (Tavani et al. 2010).

Acknowledgments

The authors would like to thank the Istituto Nazionale di Astrofisica, the Agenzia Spaziale Italiana, the Consorzio Interuniversitario per la Fisica Spaziale, and the Istituto Nazionale di Fisica Nucleare for their generous support of the AGILE mission and this research, including ASI contracts N. I/042/10/1 and I/028/12/0.

References

- Abdo, A. A., Ackermann, M., Ajello, M., et al. 2009, *ApJ*, 707, 1310
- Acero, F., Ackermann, M., Ajello, M., et al. 2015, Fermi Large Area Telescope Third Source Catalog, *Astrophysical Journal Supplement Series*, accepted [arXiv:1501.02003]
- Acero, F., Ackermann, M., Ajello, M., et al. 2013, *ApJ*, 773, 77
- Bulgarelli, A., Chen, A. W., Tavani, M., et al. 2012a, *A. & A.*, 540, A79
- Bulgarelli, A., Gianotti, F., Trifoglio, M., et al. 2010, *The Astronomer’s Telegram*, 2641
- Bulgarelli, A., Tavani, M., Chen, A. W., et al. 2012b, *A. & A.*, 538, A63
- Carosi, A., Lucarelli, F., & Antonelli, L. in press 2015, in *Proc. 34th International Cosmic Ray Conference*, The Hague, The Netherlands
- Chen, A. W., Argan, A., Bulgarelli, A., et al. 2013, *A. & A.*, 558, A37
- Chen, A. W. et al. 2011, *GRID Scientific Analysis – USER MANUAL*, http://agile.asdc.asi.it/public/AGILE_SW_5.0_SourceCode/
- Ferenc, D. 2005, *Nucl. Instrum. Methods A*, A553, 274
- Funk, S., Hinton, J. A., & CTA Consortium. 2013, *Astroparticle Physics*, 43, 348
- Funk, S., Reimer, O., Torres, D., & Hinton, J. A. 2007, in *Proceedings, 30th International Cosmic Ray Conference (ICRC 2007)*, Vol. 2, 617–620
- Funk, S., Reimer, O., Torres, D. F., & Hinton, J. A. 2008, *ApJ*, 679, 1299
- Giuliani, A., Chen, A. W., & Mereghetti, S. 2004, *Memorie della Società Astronomica Italiana Supplement*, 5, 135
- Hinton, J. 2004, *New Astron. Rev.*, 48, 331
- Holder, J. et al. 2006, *Astropart. Phys.*, 25, 391
- Longo, F. et al. 2011, TeV sources analysis with AGILE, arXiv:1111.2039 [astro-ph.HE]
- Lucarelli, F., Pittori, C., Rappoldi, A., & Longo, F. 2011, in *32nd International Cosmic Ray Conference*, Vol. 7, Beijing, China, 236
- Mattox, J., Bertsch, D., Chiang, J., et al. 1996, *ApJ*, 461, 396
- Pellizzoni, A. et al. 2010, *Science*, 327, 663
- Pittori, C. et al. 2009, *A. & A.*, 506, 1563
- Rappoldi, A. et al. 2011, *Nucl. Instrum. Methods A*, 630, 202
- Sabatini, S., Donnarumma, I., Tavani, M., et al. 2015, *ApJ*
- Striani, E., Verrecchia, F., Donnarumma, I., et al. 2010, *The Astronomer’s Telegram*, 2686
- Tavani, M., Giuliani, A., Chen, A. W., et al. 2010, *ApJ*, 710, L151
- Tavani, M. et al. 2009, *A. & A.*, 502, 995
- Verrecchia, F., Gasparrini, D., Cutini, S., et al. 2008, *The Astronomer’s Telegram*, 1582
- Verrecchia, F., Lucarelli, F., Pittori, C., et al. 2014, *The Astronomer’s Telegram*, 6733
- Verrecchia, F., Pittori, C., Chen, A. W., et al. 2013, *A. & A.*, 558, 137
- Wakely, S. and Horan, D., <http://tevcat.uchicago.edu>

Table 1. List of the 152 TeV sources considered in this analysis. The sources passing the detection criteria discussed in Sect. 5.2 are shown in bold. For a detailed description of the table columns please refer to the text.

| ID | TeV Source | (l, b) [deg] ⁸ | TeV Pos. Err. [deg] | Canonical name | Type ⁷ | $\sqrt{(TS)_4}$ | $\sqrt{(TS)_3}$ | Flux ₄ (E>100 MeV) [10 ⁻⁷ ph cm ⁻² s ⁻¹] | UL ₄ [10 ⁻⁷ ph cm ⁻² s ⁻¹] | Ext. |
|-----------|----------------------------------|--------------------------------|------------------------|------------------------|-------------------|-----------------|-----------------|--|--|----------|
| 1 | TeVJ0006+727 | 119.604, 10.403 | 0.091 | CTA 1 | PWN/SNR | 21.4 | 21.6 | 3.3±0.2 | | X |
| 2 | TeVJ0013-189 | 74.6130, -78.0684 | 0.0083 | SHBL J001355.9-185406 | HBL | | | | 1.5 | |
| 3 | TeVJ0025+640 | 120.106, 1.451 | 0.026 | Tycho SN, G120.1+1.4 | SNR | 1.6 | 1.6 | | 0.7 | |
| 4 | TeVJ0033-193 | 94.171, -81.216* | - | KUV 00311-1938 | HBL | | | | 2.0 | |
| 5 | TeVJ0035+598 | 120.898, -3.018 | 0.030 | 1ES 0033+595 | HBL | | | | 0.2 | |
| 6 | TeVJ0047-253 | 97.4696, -87.9672 | 0.0080 | NGC 253 | Sbs | | | | 0.6 | |
| 7 | TeVJ0112+227 | 129.14, -39.88* | - | S2 0109+22 | IBL | 1.8 | 3.3 | | 0.8 | |
| 8 | TeVJ0136+391 | 132.416, -22.940* | - | RGB J0136+391 | HBL | 1.2 | 1.2 | | 0.5 | |
| 9 | TeVJ0152+017 | 152.343, -57.561 | 0.030 | RGB J0152+017 | HBL | 1.9 | 3.7 | | 1.5 | |
| 10 | TeVJ0209+648 | 130.701, 3.102 | 0.059 | 3C 58 | PWN | 2.1 | 4.8 | | 0.8 | |
| 11 | TeVJ0218+359 | 142.602, -23.487 | - | S3 0218+35 | AGN | 3.3 | 3.9 | | 1.0 | |
| 12 | TeVJ0222+430⁹ | 140.143, -16.767 | - | 3C 66A | IBL | 8.0 | 8.1 | 1.4±0.2 | | |
| 13 | TeVJ0223+430 ⁹ | 140.254, -16.772 | 0.048 | MAGIC J0223+430 | UNID | 7.6 | 8.0 | 1.3±0.2 | | |
| 14 | TeVJ0232+202 | 152.970, -36.613 | 0.014 | 1ES 0229+200 | HBL | 3.1 | 4.2 | 0.9±0.3 | | |
| 15 | TeVJ0240+612 | 135.668, 1.113 | 0.034 | LSI+61_303 | XRFB | 26.7 | 27.0 | 6.5±0.3 | | |
| 16 | TeVJ0303-241 | 214.6296, -60.1899 | 0.0073 | PKS 0301-243 | HBL | | | | 0.9 | |
| 17 | TeVJ0316+413 | 150.183, -13.734 | - | IC 310 | HBL | | | | 0.3 | |
| 18 | TeVJ0319+187 | 165.088, -31.708* | 0.034 | RBS 0413 | HBL | 2.0 | | | 1.2 | |
| 19 | TeVJ0319+415 | 150.576, -13.261 | - | NGC 1275 | FRI | 5.5 | 5.5 | 1.0±0.2 | | |
| 20 | TeVJ0349-119 | 201.909, -45.704 | 0.011 | 1ES 0347-121 | HBL | | | | 0.8 | |
| 21 | TeVJ0416+010 | 191.8167, -33.1581 | 0.0069 | 1ES 0414+009 | HBL | 2.4 | 3.4 | | 1.5 | |
| 22 | TeVJ0449-438 | 248.8066, -39.9082 | 0.0072 | PKS 0447-439 | HBL | 1.3 | 1.3 | | 1.1 | |
| 23 | TeVJ0507+676 | 143.795, 15.890* | - | 1ES 0502+675 | HBL | | | | 0.2 | |
| 24 | TeVJ0521+211¹⁰ | 183.6021, -8.7114 | 0.0080 | RGB J0521.8+211 | IBL | 4.5 | 4.7 | 1.6±0.4 | | |
| 25 | TeVJ0525-696 | 280.307, -32.784* | - | LMC N132D | SNR/MC | 1.0 | 1.0 | | 0.6 | |
| 26 | TeVJ0534+220 | 184.5558, -5.7870 | 0.0070 | Crab Nebula | PWN | 55.7 | 55.9 | 26.7±0.7 | | |
| 27 | TeVJ0535-692 | 279.60, -31.91 | 0.022 | 30 Dor C | Superbubble | 3.5 | 3.8 | | 1.1 | |
| 28 | TeVJ0537-691 | 279.553, -31.750 | 0.010 | N 157B | PWN | 3.4 | 3.7 | | 1.1 | |
| 29 | TeVJ0550-322 | 237.562, -26.152 | 0.014 | PKS 0548-322 | HBL | | | | 0.6 | |
| 30 | TeVJ0616+225 | 189.073, 2.918 | 0.085 | IC 443 | SNR | 12.9 | 13.2 | 5.0±0.5 | | X |
| 31 | TeVJ0632+057 | 205.660, -1.441 | 0.010 | HESS J0632+057 | XRFB | 2.5 | 4.8 | | 1.9 | |
| 32 | TeVJ0632+173 | 195.34, 3.78 | 0.50 | Geminga PWN | PWN | 75.2 | 82.6 | 40.3±0.9 | | X |
| 33 | TeVJ0648+152 | 198.99, 6.32 | 0.12 | RX J0648.7+1516 | HBL | | | | 0.7 | |
| 34 | TeVJ0650+250 | 190.282, 10.996* | - | 1ES 0647+250 | HBL | | | | 0.6 | |
| 35 | TeVJ0710+591 | 157.391, 25.421 | 0.027 | RGB J0710+591 | HBL | | | | 0.4 | |
| 36 | TeVJ0721+713 | 143.981, 28.018* | - | S5 0716+714 | LBL | 13.8 | 13.9 | 2.6±0.2 | | |
| 37 | TeVJ0809+523 | 166.246, 32.935 | 0.048 | 1ES 0806+524 | HBL | 1.9 | 2.0 | | 0.9 | |
| 38 | TeVJ0835-455¹¹ | 263.840, -3.073 | 0.034 | Vela X | PWN | 7.9 | 11.2 | 6.2±0.8 | | X |
| 39 | TeVJ0847+115 | 215.456, 30.890* | - | RBS 0723 | HBL | | | | 0.8 | |
| 40 | TeVJ0852-463¹² | 266.285, -1.241 | - | RX J0852.0-4622 | SNR | 4.0 | 8.5 | 1.5±0.4 | | X |
| 41 | TeVJ0955+696 | 141.409, 40.568* | - | M82 | Sbs | | | | 0.3 | |
| 42 | TeVJ0958+655 | 145.75, 43.13* | - | S4 0954+65 | FSRQ | 1.8 | 1.9 | | 0.8 | |

Continued on next page

A. Rappoldi et al.: TeV sources detected by AGILE

⁷ TeV source classification types: PWN: Pulsar Wind Nebulae; BIN: Binary; SNR: SuperNova Remnant; Sbs: StarBursts; UNID: UNIDentified; FSRQ: Flat Spectrum Radio Quasar; HBL: High frequency peaked BL Lac object; IBL: Intermediate frequency peaked BL Lac object; LBL: Low frequency peaked BL Lac object; XRFB: X-Rays Binary; WR: Wolf-Rayet star; FRI: Fanaroff-Riley type I; GC: Globular Cluster; MC: Molecular Cloud; PSR: Pulsar. Note that the γ -ray emission detected in the search of counterparts to the TeV emission from PWN is in general due to the average (pulsar + nebula) γ -ray flux values. Timing analysis of pulsars was not performed in this paper.

⁸ The * indicates that the best-fit position of the TeV excess is not available and the position of the optical/radio known counterpart has been used.

⁹ The sources TeVJ0222+430 and TeVJ0223+430 are as close as 0.1° and therefore undistinguishable in this analysis. Their detection is counted as one.

¹⁰ Results of a refined MLE analysis performed using the updated AGILE best-fit position of the Crab Nebula (one of the known γ -ray sources within 10 deg from the TeV J0521+211 position) obtained in this work.

¹¹ The TeV error region for the Vela X PWN does not overlap the AGILE Vela Pulsar position error, hence the Vela PSR average γ -ray flux value for a spectral index of -1.69 was subtracted in the MLE automatic analysis. However the result is affected by the very intense nearby Vela Pulsar. The Vela X accurate γ -ray flux estimate and source location by AGILE is discussed in the dedicated analysis in (Pellizzoni et al. 2010).

¹² Also in this case, the MLE automatic analysis is affected by the very intense nearby Vela Pulsar. A dedicated analysis will be performed.

Table 1 – continued from previous page

| ID | TeV Source | (l, b) [deg] ⁹ | TeV Pos. Err. [deg] | Canonical name | Type | $\sqrt{(TS)_4}$ | $\sqrt{(TS)_3}$ | Flux ₄ (E>100 MeV) [10 ⁻⁷ ph cm ⁻² s ⁻¹] | UL ₄ [10 ⁻⁷ ph cm ⁻² s ⁻¹] | Ext. |
|----|----------------------------------|--------------------------------|------------------------|----------------------------|----------------|-----------------|-----------------|--|--|----------|
| 43 | TeVJ1010-313 | 266.896, 20.063 | 0.017 | 1RXS J101015.9-311909 | HBL | | | | 0.1 | |
| 44 | TeVJ1015+494 | 165.534, 52.712* | - | 1ES 1011+496 | HBL | 2.4 | 2.9 | | 1.2 | |
| 45 | TeVJ1018-589 | 284.256, -1.818 | - | HESS J1018-589 | BIN | 7.0 | 7.9 | 2.4±0.4 | | X |
| 46 | TeVJ1023-575 | 284.217, -0.401 | 0.030 | Westerlund 2 | WR | 2.1 | 3.5 | | 1.5 | X |
| 47 | TeVJ1026-582 | 284.798, -0.520 | 0.090 | HESS J1026-582 | PWN | | | | 0.2 | X |
| 48 | TeVJ1103-234 | 273.188, 33.074 | 0.012 | 1ES 1101-232 | HBL | | | | 0.3 | |
| 49 | TeVJ1104+382 | 179.832, 65.032 | - | Mrk 421 | HBL | 5.2 | 5.2 | 1.6±0.4 | | |
| 50 | TeVJ1119-614 | 292.102, -0.487 | - | G 292.2-0.5 | PWN | 2.3 | 4.6 | | 1.3 | X |
| 51 | TeVJ1136+676 | 133.453, 47.951* | - | RXJ1136.5+6737 | HBL | | | | 0.4 | |
| 52 | TeVJ1136+701 | 131.910, 45.641* | - | Mrk 180 | HBL | 1.4 | 1.4 | | 0.7 | |
| 53 | TeVJ1217+301 | 189.010, 82.046 | 0.016 | 1ES 1215+303 | HBL | | | | 0.3 | |
| 54 | TeVJ1221+282 ¹³ | 201.734, 83.288 | - | W Comae | IBL | | | | 1.0 | |
| 55 | TeVJ1221+301 | 186.210, 82.743 | 0.031 | 1ES 1218+304 | HBL | | | | 0.2 | |
| 56 | TeVJ1224+213 ¹⁴ | 255.074, 81.660* | - | 4C +21.35 | FSRQ | 2.6 | 3.5 | | 1.7 | |
| 57 | TeVJ1224+246 | 233.952, 83.418 | - | MS 1221.8+2452 | HBL | | | | 0.7 | |
| 58 | TeVJ1230+123 | 283.7388, 74.4946* | 0.0080 | M 87 | FRI | | | | 1.0 | |
| 59 | TeVJ1230+253 | 232.75, 84.91* | - | S3 1227+25 | IBL | 2.8 | 3.0 | | 1.7 | |
| 60 | TeVJ1256-057 | 305.104, 57.062* | - | 3C 279 | FSRQ | 11.1 | 11.2 | 4.2±0.5 | | |
| 61 | TeVJ1302-638 | 304.187, -0.987 | 0.011 | PSR B1259-63 | XRB | | | | 0.6 | |
| 62 | TeVJ1303-631 | 304.213, -0.334 | 0.014 | HESS J1303-631 | PWN | | | | 0.4 | X |
| 63 | TeVJ1315-426 | 307.540, 20.064 | 0.018 | 1ES 1312-423 | HBL | 2.4 | 5.1 | | 0.9 | |
| 64 | TeVJ1325-430¹⁵ | 309.513, 19.425 | 0.021 | Centaurus A | FRI | 4.4 | 4.9 | 0.8±0.2 | | |
| 65 | TeVJ1356-645 | 309.812, -2.494 | 0.034 | HESS J1356-645 | PWN | 1.7 | 2.0 | | 1.0 | X |
| 66 | TeVJ1418-609 | 313.247, 0.150 | 0.030 | Kookaburra (Rabbit) | PWN | 13.5 | 13.5 | 5.1±0.4 | | X |
| 67 | TeVJ1420-607 | 313.558, 0.268 | 0.018 | Kookaburra (PWN) | PWN | | | | 1.1 | X |
| 68 | TeVJ1427+238 | 29.472, 68.208 | 0.033 | PKS 1424+240 | IBL | 1.3 | 1.3 | | 1.3 | |
| 69 | TeVJ1427-608 | 314.408, -0.145 | 0.050 | HESS J1427-608 | UNID | 1.2 | 1.2 | | 1.1 | |
| 70 | TeVJ1428+426 | 77.487, 64.899* | - | H 1426+428 | HBL | | | | 1.0 | X |
| 71 | TeVJ1442-624 | 315.410, -2.300 | 0.059 | RCW 86 | SNR | | | | 0.5 | X |
| 72 | TeVJ1443+120 | 8.330, 59.840* | - | 1ES 1440+122 | IBL | | | | 0.6 | |
| 73 | TeVJ1443+250 | 34.56, 64.70* | - | PKS 1441+25 | FSRQ | | | | 0.7 | |
| 74 | TeVJ1457-594 | 318.36, -0.43 | 0.14 | G 318.2+0.1 | SNR/MC | | | | 0.2 | X |
| 75 | TeVJ1459-608 | 317.748, -1.704 | 0.030 | HESS J1458-608 | PWN | 5.6 | 5.8 | 1.5±0.3 | | X |
| 76 | TeVJ1502-419 | 327.580, 14.571 | - | SN 1006 | SNR | | | | 0.3 | |
| 77 | TeVJ1503-582 | 319.62, 0.29 | 0.10 | HESS J1503-582 | UNID | | | | 0.2 | X |
| 78 | TeVJ1506-623 | 317.946, -3.494 | 0.050 | HESS J1507-622 | UNID | 3.1 | 4.3 | | 1.2 | X |
| 79 | TeVJ1512-091 | 351.2907, 40.1296 | 0.0093 | PKS 1510-089 | FSRQ | 24.8 | 25.0 | 8.1±0.4 | | X |
| 80 | TeVJ1514-591 | 320.324, -1.200 | 0.010 | MSH 15-52 | PWN | | | | 0.6 | X |
| 81 | TeVJ1517-243 | 340.673, 27.577* | 0.014 | AP Lib | LBL | 2.0 | 3.6 | | 0.8 | |
| 82 | TeVJ1554-550 | 327.158, -1.072 | 0.018 | G 327.1-1.1 | PWN | | | | 0.3 | X |
| 83 | TeVJ1555+111 | 21.919, 43.960 | 0.016 | PG 1553+113 | HBL | 1.9 | 4.4 | | 1.3 | |
| 84 | TeVJ1614-518 | 331.52, -0.58 | - | HESS J1614-518 | UNID | | | | 0.8 | X |
| 85 | TeVJ1616-508 | 332.39, -0.14 | - | HESS J1616-508 | PWN | | | | 0.9 | X |
| 86 | TeVJ1626-490 | 334.772, 0.045 | 0.050 | HESS J1626-490 | UNID | | | | 0.3 | |
| 87 | TeVJ1632-478¹⁶ | 336.38, 0.19 | - | HESS J1632-478 | UNID | 5.6 | 5.7 | 2.2±0.4 | | X |
| 88 | TeVJ1634-472 | 337.11, 0.22 | - | HESS J1634-472 | UNID | 15.4 | 15.7 | 6.3±0.4 | | X |
| 89 | TeVJ1640-465 | 338.32, -0.02 | - | HESS J1640-465 | PWN | 12.3 | 15.2 | 5.1±0.5 | | X |
| 90 | TeVJ1641-463 | 338.519, 0.095 | 0.015 | HESS J1641-463 | UNID | | | | 1.0 | |
| 91 | TeVJ1647-458 | 339.55, -0.35 | 0.12 | Westerlund 1 | WR | 1.3 | 1.3 | | 1.3 | X |
| 92 | TeVJ1653+397 | 63.600, 38.859 | - | Mrk 501 | HBL | 3.9 | 5.3 | | 1.3 | |
| 93 | TeVJ1702-420 | 344.304, -0.184 | 0.050 | HESS J1702-420 | UNID | | | | 0.2 | X |
| 94 | TeVJ1708-410 | 345.683, -0.469 | 0.050 | HESS J1708-410 | UNID | | | | 0.4 | X |
| 95 | TeVJ1708-443 | 343.058, -2.376 | 0.071 | HESS J1708-443 | PWN/SNR | 39.8 | 42.3 | 13.6±0.4 | | X |
| 96 | TeVJ1713-382 | 348.639, 0.388 | 0.018 | CTB 37B | SNR | 6.5 | 7.8 | 2.6±0.4 | | X |

Continued on next page

A. Rappoldi et al.: TeV sources detected by AGILE

¹³ Detected by AGILE during a flaring episode (Verrecchia et al. 2008).¹⁴ Detected by AGILE during several flaring episodes (Bulgarelli et al. 2010; Striani et al. 2010; Verrecchia et al. 2014).¹⁵ The region of the MLE analysis is not yet well modelled since this source shows a point-like core and extended emission from the lobes, which are not yet included in the AGILE reference Catalogs. A dedicated analysis will be performed.¹⁶ AGILE detection presented at the 32nd ICRC (Lucarelli et al. 2011).

Table 1 – continued from previous page

| ID | TeV Source | (l, b) [deg] ⁹ | TeV Pos. Err. [deg] | Canonical name | Type | $\sqrt{(TS)_4}$ | $\sqrt{(TS)_3}$ | Flux ₄ (E>100 MeV) [10 ⁻⁷ ph cm ⁻² s ⁻¹] | UL ₄ [10 ⁻⁷ ph cm ⁻² s ⁻¹] | Ext. |
|-----|----------------------------|--------------------------------|------------------------|------------------------|--------|-----------------|-----------------|--|--|------|
| 97 | TeVJ1713-397 | 347.336, -0.473 | - | RX J1713.7-3946 | SNR | 3.7 | 7.0 | | 2.2 | X |
| 98 | TeVJ1714-385 ¹⁷ | 348.389, 0.107 | 0.023 | CTB 37A | SNR | 7.0 | 7.5 | 2.8±0.4 | | X |
| 99 | TeVJ1718-374 | 349.720, 0.174 | 0.010 | G 349.7+0.2 | SNR/MC | 6.2 | 7.6 | 2.6±0.4 | | |
| 100 | TeVJ1718-385 | 348.834, -0.488 | 0.034 | HESS J1718-385 | PWN | 6.9 | 7.5 | 2.7±0.4 | | X |
| 101 | TeVJ1725+118 | 34.120, 24.475* | - | H 1722+119 | HBL | | | | 0.4 | |
| 102 | TeVJ1728+502 | 77.068, 33.537 | - | 1ES 1727+502 | HBL | | | | 0.4 | |
| 103 | TeVJ1729-345 | 353.444, -0.128 | 0.035 | HESS J1729-345 | UNID | 8.0 | 10.3 | 3.6±0.5 | | X |
| 104 | TeVJ1732-347 ¹⁶ | 353.542, -0.670 | - | HESS J1731-347 | SNR | 7.3 | 10.2 | 3.1±0.5 | | X |
| 105 | TeVJ1741-302 ¹⁸ | 358.397, 0.191 | - | HESS J1741-302 | UNID | 4.3 | 9.6 | 2.1±0.5 | | |
| 106 | TeVJ1743+196 | 43.836, 23.339* | - | 1ES 1741+196 | HBL | | | | 0.3 | |
| 107 | TeVJ1745-290 | 359.9449, -0.0440 | 0.0024 | HESS J1745-290 | UNID | | | | 0.3 | |
| 108 | TeVJ1745-303 | 358.710, -0.640 | - | HESS J1745-303 | SNR/MC | 11.2 | 12.7 | 5.5±0.5 | | X |
| 109 | TeVJ1747-248 | 3.78, 1.72 | 0.45 | Terzan 5 | GC | 5.2 | 5.9 | 1.9±0.4 | | X |
| 110 | TeVJ1747-281 | 0.872, 0.076 | - | G 0.9+0.1 | PWN | | | | 0.1 | |
| 111 | TeVJ1800-240 | 5.960, -0.380 | 0.044 | HESS J1800-240 (A+B+C) | UNID | | | | 0.9 | X |
| 112 | TeVJ1801-233 | 6.657, -0.268 | 0.032 | W28 | SNR/MC | 14.0 | 15.0 | 6.5±0.5 | | X |
| 113 | TeVJ1804-216 | 8.354, -0.000 | - | HESS J1804-216 | UNID | 7.5 | 7.8 | 3.4±0.5 | | X |
| 114 | TeVJ1808-204 | 9.960, -0.248 | 0.038 | HESS J1808-204 | UNID | | | | 1.3 | |
| 115 | TeVJ1809-193 | 11.180, -0.088 | 0.050 | HESS J1809-193 | PWN | 3.4 | 4.1 | | 2.4 | X |
| 116 | TeVJ1813-178 | 12.812, -0.026 | - | HESS J1813-178 | PWN | 4.1 | 4.8 | 1.9±0.5 | | X |
| 117 | TeVJ1818-154 | 15.409, 0.161 | 0.014 | G 15.4+0.1 | PWN | 1.8 | 9.0 | | 1.7 | X |
| 118 | TeVJ1825-137 | 17.711, -0.697 | 0.018 | HESS J1825-137 | PWN | 8.0 | 11.3 | 3.8±0.5 | | X |
| 119 | TeVJ1826-148 ¹⁷ | 16.902, -1.278 | 0.012 | LS 5039 | XRB | 7.7 | 10.7 | 3.3±0.5 | | |
| 120 | TeVJ1831-099 | 21.850, -0.109 | - | HESS J1831-098 | PWN | 1.9 | 4.2 | | 1.8 | X |
| 121 | TeVJ1832-093 | 22.476, -0.177 | 0.015 | G 22.7-0.2 | SNR/MC | 1.1 | 1.1 | | 1.4 | X |
| 122 | TeVJ1833-106 | 21.511, -0.876 | 0.016 | HESS J1833-105 | UNID | 2.3 | 3.6 | | 1.8 | |
| 123 | TeVJ1834-087 | 23.24, -0.32 | - | HESS J1834-087 | UNID | | | | 0.9 | X |
| 124 | TeVJ1837-069 | 25.18, -0.11 | - | HESS J1837-069 | UNID | 4.9 | 7.4 | 2.1±0.4 | | X |
| 125 | TeVJ1841-055 ¹⁶ | 26.795, -0.198 | 0.050 | HESS J1841-055 | UNID | 12.4 | 14.0 | 5.0±0.4 | | X |
| 126 | TeVJ1843-030 | 29.033, 0.370 | - | HESS J1843-033 | UNID | 3.6 | 6.7 | | 2.2 | |
| 127 | TeVJ1846-029 | 29.705, -0.240 | 0.011 | HESS J1846-029 | PWN | 1.6 | 1.6 | | 1.5 | |
| 128 | TeVJ1848-017 | 31.000, -0.160 | - | WR121a/W43 | WR | 3.7 | 4.6 | 1.4±0.4 | | X |
| 129 | TeVJ1849-000 | 32.638, 0.526 | - | IGR J18490-0000 | PWN | | | | 1.0 | |
| 130 | TeVJ1857+026 | 36.003, -0.061 | 0.039 | HESS J1857+026 | UNID | | | | 0.2 | X |
| 131 | TeVJ1858+020 | 35.578, -0.581 | 0.050 | HESS J1858+020 | UNID | | | | 0.1 | X |
| 132 | TeVJ1907+062 | 40.280, -0.688 | 0.020 | MGRO J1908+06 | UNID | 12.9 | 13.3 | 4.5±0.4 | | X |
| 133 | TeVJ1911+090 | 43.259, -0.189 | 0.071 | W 49B | SNR/MC | 7.6 | 7.8 | 2.4±0.3 | | |
| 134 | TeVJ1912+101 | 44.391, -0.071 | 0.050 | HESS J1912+101 | PWN | 4.1 | 7.6 | 1.3±0.3 | | X |
| 135 | TeVJ1923+141 | 49.116, -0.365 | 0.015 | W 51 | SNR/MC | 7.0 | 7.1 | 2.1±0.3 | | X |
| 136 | TeVJ1930+188 | 54.10, 0.26 | 0.11 | G 54.1+0.3 | PWN | 3.5 | 5.2 | | 1.5 | |
| 137 | TeVJ1943+213 | 57.7577, -1.2928 | 0.0073 | HESS J1943+213 | HBL | | | | 0.5 | |
| 138 | TeVJ1959+651 | 98.003, 17.670* | - | 1ES 1959+650 | HBL | 3.4 | 3.7 | | 0.7 | |
| 139 | TeVJ2001+438 | 79.071, 7.110 | - | MAGIC J2001+435 | HBL | 4.9 | 4.8 | 0.9±0.2 | | |
| 140 | TeVJ2009-488 | 350.3741, -32.6052 | 0.0083 | PKS 2005-489 | HBL | | | | 0.4 | |
| 141 | TeVJ2016+372 | 74.940, 1.140 | 0.019 | VER J2016+372 | UNID | | | | 0.3 | |
| 142 | TeVJ2019+368 | 74.828, 0.417 | 0.090 | MGRO J2019+37 | PWN | 24.7 | 25.5 | 6.7±0.3 | | X |
| 143 | TeVJ2019+407 | 78.331, 2.489 | 0.035 | VER J2019+407 | UNID | | | | 0.1 | X |
| 144 | TeVJ2032+415 | 80.279, 1.042 | 0.044 | TeV J2032+4130 | UNID | 7.6 | 8.0 | 2.2±0.3 | | X |
| 145 | TeVJ2158-302 | 17.737, -52.247 | - | PKS 2155-304 | HBL | 4.6 | 4.8 | 1.3±0.3 | | |
| 146 | TeVJ2202+422 | 92.590, -10.441 | - | BL Lacertae | LBL | 7.2 | 8.0 | 1.0±0.2 | | |
| 147 | TeVJ2227+608 | 106.35, 2.71 | 0.10 | G 106.3+2.7 | SNR | 15.2 | 16.7 | 3.0±0.2 | | X |
| 148 | TeVJ2243+203 | 86.567, -33.365* | - | RGB J2243+203 | HBL | | | | 0.4 | |
| 149 | TeVJ2250+384 | 98.254, -18.578 | - | B3 2247+381 | HBL | | | | 0.2 | |
| 150 | TeVJ2323+588 | 111.735, -2.130 | 0.020 | Cassiopeia A | SNR | 5.2 | 7.2 | 0.9±0.2 | | |
| 151 | TeVJ2347+517 | 112.73, -9.86 | 0.10 | 1ES 2344+514 | HBL | | | | 0.3 | |
| 152 | TeVJ2359-306 | 12.8689, -78.0367 | 0.0086 | H 2356-309 | HBL | 3.9 | 4.0 | 3.3±1.0 | | |

A. Rappoldi et al.: TeV sources detected by AGILE

¹⁷ Source located in a crowded region of the Galactic Plane. The automatic MLE analysis is not reliable. A dedicated analysis will be performed.¹⁸ Source located in the region near the Galactic Center. The automatic MLE analysis is not reliable. A dedicated analysis is being performed with an improved AGILE diffuse background model in the Galactic Center region (Fioretti et al., in preparation).

Table 2. Results for all the sources detected with AGILE in this work, according to the criteria described in the text. The upper part reports the results of the MLE analysis *step 3*, and the lower part the results of the *step 4*.

| ID | TeV Source | $\sqrt{(TS)}$ | (l, b) [deg] | Error (95%) ¹⁹ [deg] | Flux ($E > 100$ MeV) [10^{-7} ph cm $^{-2}$ s $^{-1}$] | Dist. [deg] | AGILE Association | Fermi Association | Analysis Flag |
|-----|----------------------------|---------------|-------------------|------------------------------------|--|----------------|----------------------|--|------------------|
| 1 | TeVJ0006+727 | 21.6 | 119.66, 10.51 | 0.09 | 3.3 ± 0.2 | 0.1 | 1AGLR J0007+7307 | 3FGL J0007.0+7302 (E) | IN |
| 12 | TeVJ0222+430 | 8.1 | 140.0, -16.7 | 0.2 | 1.4 ± 0.2 | 0.1 | 1AGLR J0222+4305 | 3FGL J0222.6+4301 (P) | IN |
| 14 | TeVJ0232+202 | 4.2 | 152.9, -36.3 | 0.6 | 1.1 ± 0.3 | 0.4 | - | 3FGL J0232.8+2016 (P) | IN |
| 15 | TeVJ0240+612 | 27.1 | 135.5, 1.2 | 0.1 | 6.6 ± 0.3 | 0.2 | 1AGLR J0240+6115 | 3FGL J0240.5+6113 (P) | E |
| 19 | TeVJ0319+415 | 5.5 | 150.6, -13.2 | 0.4 | 1.0 ± 0.2 | 0.1 | 1AGLR J0321+4137 | 3FGL J0319.8+4130 (P) | IN |
| 24 | TeVJ0521+211 | 4.7 | 183.6, -8.6 | 0.5 | 1.7 ± 0.4 | 0.1 | - | 3FGL J0521.7+2113 (P) | IN |
| 26 | TeVJ0534+220 | 55.9 | 184.48, -5.81 | 0.06 | 26.7 ± 0.7 | 0.1 | 1AGL J0535+2205 | 3FGL J0534.5+2201 (P) | IN |
| 30 | TeVJ0616+225 | 13.2 | 188.9, 3.0 | 0.2 | 5.0 ± 0.5 | 0.2 | 1AGL J0617+2236 | 3FGL J0617.2+2234e (E) | O |
| 32 | TeVJ0632+173 | 82.6 | 195.09, 4.28 | 0.04 | 41.8 ± 0.9 | 0.6 | 1AGL J0634+1748 | 3FGL J0633.9+1746 (E) | IN |
| 36 | TeVJ0721+713 | 13.9 | 143.9, 28.1 | 0.1 | 2.6 ± 0.2 | 0.1 | 1AGLR J0723+7121 | 3FGL J0721.9+7120 (P) | IN |
| 45 | TeVJ1018-589 | 7.8 | 284.0, -2.0 | 0.3 | 2.6 ± 0.4 | 0.3 | 1AGLR J1018-5852 | { 3FGL J1018.9-5856 (E) 3FGL J1016.3-5858 (E) | O |
| 49 | TeVJ1104+382 | 5.2 | 179.7, 65.0 | 0.2 | 1.6 ± 0.4 | 0.1 | 1AGLR J1105+3818 | 3FGL J1104.4+3812 (P) | IN |
| 60 | TeVJ1256-057 | 11.2 | 305.3, 57.1 | 0.2 | 4.2 ± 0.5 | 0.1 | 1AGL J1256-0549 | 3FGL J1256.1-0547 (P) | IN |
| 66 | TeVJ1418-609 | 13.5 | 313.2, 0.1 | 0.1 | 5.1 ± 0.4 | 0.1 | 1AGLR J1417-6108 | 3FGL J1418.6-6058 (E) | IN |
| 75 | TeVJ1459-608 | 5.8 | 317.6, -1.7 | 0.3 | 1.6 ± 0.3 | 0.1 | - | { 3FGLJ1456.7-6046 (E) 3FGLJ1459.4-6053 (E) | IN |
| 79 | TeVJ1512-091 | 25.0 | 351.4, 40.1 | 0.1 | 8.2 ± 0.4 | 0.1 | 1AGLR J1513-0906 | 3FGL J1512.8-0906 (P) | IN |
| 87 | TeVJ1632-478 | 5.7 | 336.4, 0.0 | 0.4 | 2.2 ± 0.4 | 0.2 | - | 3FGL J1633.0-4746e (E) | IN |
| 88 | TeVJ1634-472 | 15.2 | 337.4, 0.1 | 0.2 | 5.1 ± 0.5 | 0.3 | 1AGL J1639-4702 | - | O |
| 95 | TeVJ1708-443 | 42.3 | 343.12, -2.69 | 0.06 | 13.9 ± 0.4 | 0.3 | 1AGL J1709-4428 | 3FGL J1709.7-4429 (E) | O |
| 109 | TeVJ1747-248 | 5.9 | 4.0, 1.7 | 0.3 | 2.1 ± 0.4 | 0.2 | - | 3FGL J1748.0-2447 (E) | O |
| 112 | TeVJ1801-233 | 15.0 | 6.6, 0.1 | 0.2 | 6.8 ± 0.5 | 0.4 | 1AGL J1801-2317 | 3FGL J1801.3-2326e (E) | E |
| 113 | TeVJ1804-216 | 7.8 | 8.4, 0.2 | 0.3 | 3.5 ± 0.5 | 0.2 | 1AGLR J1805-2149 | 3FGL J1805.6-2136e (E) | O |
| 116 | TeVJ1813-178 | 4.8 | 13.0, 0.4 | 0.4 | 2.1 ± 0.5 | 0.4 | 1AGL J1815-1732 | - | IN |
| 125 | TeVJ1841-055 | 14.0 | 26.3, 0.1 | 0.2 | 5.8 ± 0.5 | 0.6 | 1AGLR J1839-0550 | 3FGL J1840.9-0532e (E) | O |
| 128 | TeVJ1848-017 | 4.6 | 30.8, 0.1 | 0.2 | 1.8 ± 0.4 | 0.4 | - | 3FGL J1848.4-0141 (E) | O |
| 132 | TeVJ1907+062 | 13.3 | 40.4, -1.0 | 0.1 | 4.4 ± 0.4 | 0.2 | 1AGL J1908+0614 | 3FGL J1907.9+0602 (E) | O |
| 133 | TeVJ1911+090 | 7.8 | 43.3, 0.0 | 0.3 | 2.4 ± 0.3 | 0.2 | - | - | IN |
| 135 | TeVJ1923+141 | 7.1 | 49.2, -0.5 | 0.3 | 2.1 ± 0.3 | 0.2 | 1AGL J1923+1404 | 3FGL J1923.2+1408e (E) | IN |
| 142 | TeVJ2019+368 | 25.5 | 75.17, 0.25 | 0.09 | 6.9 ± 0.3 | 0.2 | 1AGLR J2021+3653 | 3FGL J2021.1+3651 (E) | IN |
| 144 | TeVJ2032+415 | 8.0 | 80.3, 1.2 | 0.2 | 2.3 ± 0.3 | 0.1 | 1AGLR J2031+4130 | 3FGL J2032.2+4126 (E) | O |
| 145 | TeVJ2158-302 | 4.8 | 17.6, -52.0 | 0.6 | 1.4 ± 0.3 | 0.3 | - | 3FGLJ2158.8-3013 (P) | IN |
| 147 | TeVJ2227+608 | 16.7 | 106.7, 3.0 | 0.2 | 3.3 ± 0.2 | 0.4 | 1AGL J2231+6109 | 3FGL J2225.8+6045 (E) | E |
| 152 | TeVJ2359-306 | 4.0 | 12.6, -78.0 | 0.3 | 3.3 ± 1.0 | 0.1 | - | 3FGL J2359.3-3038 (P) | IN |
| 38 | TeVJ0835-455 ¹¹ | 7.9 | -, - | - | 6.2 ± 0.8 | - | - | 3FGL J0833.1-4511e (E) | - |
| 40 | TeVJ0852-463 ¹² | 4.0 | -, - | - | 1.5 ± 0.4 | - | - | 3FGL J0852.7-4631e (E) | - |
| 64 | TeVJ1325-430 ¹⁵ | 4.4 | -, - | - | 0.8 ± 0.2 | - | - | 3FGL J1325.4-4301 (P) | - |
| 89 | TeVJ1640-465 | 12.3 | -, - | - | 5.1 ± 0.5 | - | 1AGL J1639-4702 | 3FGL J1640.4-4634c (E) | - |
| 96 | TeVJ1713-382 | 6.5 | -, - | - | 2.6 ± 0.4 | - | - | - | - |
| 98 | TeVJ1714-385 ¹⁷ | 7.0 | -, - | - | 2.8 ± 0.4 | - | - | 3FGL J1714.5-3832 (E) | - |
| 99 | TeVJ1718-374 | 6.2 | -, - | - | 2.6 ± 0.4 | - | - | 3FGL J1718.0-3726 (P) | - |
| 100 | TeVJ1718-385 | 6.9 | -, - | - | 2.7 ± 0.4 | - | - | 3FGL J1718.1-3825 (E) | - |
| 103 | TeVJ1729-345 | 8.0 | -, - | - | 3.6 ± 0.5 | - | - | - | - |
| 104 | TeVJ1732-347 | 7.3 | -, - | - | 3.1 ± 0.5 | - | - | - | - |
| 105 | TeVJ1741-302 ¹⁸ | 4.3 | -, - | - | 2.1 ± 0.5 | - | - | - | - |
| 108 | TeVJ1745-303 | 11.2 | -, - | - | 5.5 ± 0.5 | - | 1AGL J1746-3017 | 3FGL J1745.1-3011 (E) | - |
| 118 | TeVJ1825-137 | 8.0 | -, - | - | 3.8 ± 0.5 | - | - | 3FGL J1824.5-1351e (E) | - |
| 119 | TeVJ1826-148 ¹⁷ | 7.7 | -, - | - | 3.3 ± 0.5 | - | - | 3FGL J1826.2-1450 (P) | - |
| 124 | TeVJ1837-069 | 4.9 | -, - | - | 2.1 ± 0.4 | - | - | 3FGL J1836.5-0655e (E) | - |
| 134 | TeVJ1912+101 | 4.1 | -, - | - | 1.3 ± 0.3 | - | - | - | - |
| 139 | TeVJ2001+438 | 4.9 | -, - | - | 0.9 ± 0.2 | - | - | 3FGL J2001.1+4352 (P) | - |
| 146 | TeVJ2202+422 | 7.2 | -, - | - | 1.0 ± 0.2 | - | - | 3FGL J2202.7+4217 (P) | - |
| 150 | TeVJ2323+588 | 5.2 | -, - | - | 0.9 ± 0.2 | - | - | 3FGL J2323.4+5849 (P) | - |

A. Rappoldi et al.: TeV sources detected by AGILE

¹⁹ The AGILE Team recommends to add linearly a systematic error of $\pm 0.1^\circ$.

Table 3. Results of the spectral analysis of the most significant sources detected with AGILE in this analysis. The spectral indexes for all sources detected with a significance $\sqrt{(TS)_3} > 5$ (see upper part of Table 2) and Galactic latitude $|b| < 30^\circ$ are reported. The last column shows the Fermi *power-law index* as given in the indicated reference; when the Fermi sources spectrum has been fitted with a *power-law* function (i.e. the spectral form is **PowerLaw**), the corresponding error is also available and reported.

| ID | TeV Source | Type | AGILE power-law spectral index ²⁰ | AGILE Association | Fermi Association | 3FGL power-law spectral index ²¹ |
|-----|--------------|--------|--|-------------------|--|---|
| 1 | TeVJ0006+727 | PWN | 1.91 ± 0.05 | 1AGLR J0007+7307 | 3FGL J0007.0+7302 | 1.88 |
| 12 | TeVJ0222+430 | IBL | 2.04 ± 0.10 | 1AGLR J0222+4305 | 3FGL J0222.6+4301 | 1.94 |
| 15 | TeVJ0240+612 | XRB | 2.19 ± 0.04 | 1AGLR J0240+6115 | 3FGL J0240.5+6113 | 2.29 |
| 19 | TeVJ0319+415 | FRI | 1.80 ± 0.14 | 1AGLR J0321+4137 | 3FGL J0319.8+4130 | 2.08 |
| 26 | TeVJ0534+220 | PWN | 2.27 ± 0.03 | 1AGL J0535+2205 | 3FGL J0534.5+2201 | 2.23 |
| 30 | TeVJ0616+225 | SNR | 1.95 ± 0.07 | 1AGL J0617+2236 | 3FGL J0617.2+2234e | 1.98 |
| 32 | TeVJ0632+173 | PWN | 1.88 ± 0.02 | 1AGL J0634+1748 | 3FGL J0633.9+1746 | 1.87 |
| 36 | TeVJ0721+713 | LBL | 1.87 ± 0.07 | 1AGLR J0723+7121 | 3FGL J0721.9+7120 | 2.04 |
| 45 | TeVJ1018-589 | BIN | 2.07 ± 0.11 | 1AGLR J1018-5852 | { 3FGL J1016.3-5858 3FGL J1018.9-5856 | { 2.35 2.30 |
| 66 | TeVJ1418-609 | PWN | 2.00 ± 0.07 | 1AGLR J1417-6108 | 3FGL J1418.6-6058 | 2.27 |
| 75 | TeVJ1459-608 | PWN | 2.16 ± 0.12 | - | { 3FGL J1456.7-6046 3FGL J1459.4-6053 | { 2.37 2.37 |
| 87 | TeVJ1632-478 | UNID | 2.05 ± 0.14 | - | 3FGL J1633.0-4746e | 2.11 ± 0.02 |
| 88 | TeVJ1634-472 | UNID | 2.58 ± 0.08 | 1AGL J1639-4702 | - | - |
| 95 | TeVJ1708-443 | PWN | 2.02 ± 0.02 | 1AGL J1709-4428 | 3FGL J1709.7-4429 | 2.02 |
| 109 | TeVJ1747-248 | GC | 1.99 ± 0.17 | - | 3FGL J1748.0-2447 | 2.26 |
| 112 | TeVJ1801-233 | SNR/MC | 2.07 ± 0.07 | 1AGL J1801-2317 | 3FGL J1801.3-2326e | 2.15 |
| 113 | TeVJ1804-216 | UNID | 2.13 ± 0.12 | 1AGLR J1805-2149 | 3FGL J1805.6-2136e | 2.07 |
| 125 | TeVJ1841-055 | UNID | 2.41 ± 0.08 | 1AGLR J1839-0550 | 3FGL J1840.9-0532e | 1.81 ± 0.04 |
| 132 | TeVJ1907+062 | UNID | 2.36 ± 0.07 | 1AGL J1908+0614 | 3FGL J1907.9+0602 | 2.24 |
| 133 | TeVJ1911+090 | SNR/MC | 2.21 ± 0.12 | - | - | - |
| 135 | TeVJ1923+141 | SNR/MC | 2.23 ± 0.12 | 1AGL J1923+1404 | 3FGL J1923.2+1408e | 2.15 |
| 142 | TeVJ2019+368 | PWN | 1.98 ± 0.04 | 1AGLR J2021+3653 | 3FGL J2021.1+3651 | 2.17 |
| 144 | TeVJ2032+415 | UNID | 2.05 ± 0.10 | 1AGLR J2031+4130 | 3FGL J2032.2+4126 | 2.08 |
| 147 | TeVJ2227+608 | SNR | 2.30 ± 0.06 | 1AGL J2231+6109 | 3FGL J2225.8+6045 | 1.95 ± 0.20 |

²⁰ This analysis.

²¹ (Acero et al. 2015). The errors on the Fermi power-law spectral indices in the 3FGL catalog are available only for three sources: 3FGL J1633.0-4746e, 3FGL J1840.9-0532e, 3FGL J2225.8+6045. See also footnote ⁵.

Table 4. Statistics about the sources detected by AGILE in this work, grouped by source type classification. Enclosed in parenthesis, the percentage of detected sources with respect to the total class sample.

| <i>Source type</i> | <i>Detected / Total</i> | <i>Source class</i> | <i>Detected / Total</i> |
|--------------------|-------------------------|---------------------|-------------------------|
| EXTRAGALACTIC | 13 / 66 (20%) | Blazar | 0 / 1 (0%) |
| | | HBL | 5 / 44 (11%) |
| | | IBL | 2 / 7 (29%) |
| | | LBL | 2 / 3 (67%) |
| | | FSRQ | 2 / 5 (40%) |
| | | Sbs | 0 / 2 (0%) |
| | | Superbubble | 0 / 1 (0%) |
| | | FRI | 2 / 3 (67%) |
| GALACTIC | 30 / 58 (52%) | PWN | 11 / 28 (39%) |
| | | SNR | 7 / 11 (64%) |
| | | PWN/SNR | 2 / 2 (100%) |
| | | SNR/MC | 5 / 8 (63%) |
| | | BIN/XRB | 3 / 5 (60%) |
| | | GC | 1 / 1 (100%) |
| | | WR | 1 / 3 (33%) |
| UNIDENTIFIED | 9 / 28 (32%) | - | - |